Atherosclerosis 289 (2019) 132–142

Contents lists available at ScienceDirect

Atherosclerosis

journal homepage: www.elsevier.com/locate/atherosclerosis

Inhibition of vascular neointima hyperplasia by FGF21 associated with FGFR1/Syk/NLRP3 inflammasome pathway in diabetic mice

Wei Wei[a], Xiao-Xue Li[b], Ming Xu[a,*]

[a] Department of Clinical Pharmacy, School of Preclinical Medicine and Clinical Pharmacy, China Pharmaceutical University, Nanjing, 210009, China
[b] Department of Pharmacology, Southeast University School of Medicine, Nanjing, 210009, China

HIGHLIGHTS

- FGF21 attenuated neointima hyperplasia in wire-injured common carotid artery (CCA) of diabetic mice.
- FGF21 suppressed the proliferation and migration in high glucose-treated vascular smooth muscle cells (VSMCs).
- NLRP3 inflammasome was associated with the regulation of FGF21 in VSMCs remodeling.

ARTICLE INFO

Keywords:
FGF21
Diabetes
Neointima hyperplasia
Vascular smooth muscle cell
NLRP3 inflammasome

ABSTRACT

Background and aims: Neointima hyperplasia is the pathological basis of atherosclerosis and restenosis, which have been associated with diabetes mellitus (DM). Fibroblast growth factor 21 (FGF21) is a potential diabetic drug, however, it has not been investigated whether FGF21 prevents neointima hyperplasia in DM.

Methods: Vascular neointima hyperplasia was induced in mice fed a high fat diet (HFD) combined with low dose streptozotocin (STZ) administration. *In vitro*, vascular smooth muscle cells (VSMCs) were incubated with high glucose (HG, 30 mM). VSMC proliferation and migration, as well as formation of NLRP3 inflammasome, were assessed.

Results: We found that FGF21 significantly inhibited neointima hyperplasia and improved endothelium-independent contraction in the wire-injured common carotid artery (CCA) of diabetic mice. *In vitro*, the proliferation and migration of HG-treated VSMCs were shown as remarkable increase of PCNA, cyclin D1, MMP2 and MMP9, as well as cell migration through wound healing and transwell migration assays. Such abnormal changes were dramatically reversed by FGF21, which mimicked the role of NLRP3 inflammasome inhibitor MCC950 and caspase-1 inhibitor WEHD. Moreover, along with more NLRP3, ASC oligomer and their colocalization, the release of active caspase-1(p20) and IL-1β was significantly inhibited by FGF21 in VSMCs exposed to HG. Furthermore, FGF21 suppressed phosphorylation of spleen tyrosine kinase (Syk) via FGFR1, which regulated NLRP3 inflammasome through ASC phosphorylation and oligomerization.

Conclusions: We demonstrated that potential protection of FGF21 on VSMCs proliferation and migration was associated with inhibition of FGFR1/Syk/NLRP3 inflammasome, resulting in the improvement of neointima hyperplasia in diabetic mice.

1. Introduction

Diabetes has been associated with increased risk of atherosclerosis and restenosis after percutaneous coronary intervention (PCI) such as angioplasty and stenting [1]. Vascular neointimal formation is the pathological basis of atherosclerosis and restenosis. However, no adequate treatment modalities are available to prevent or treat the development of neointimal formation due to unknown pathogenetic mechanisms. Our study attempted to assess pharmacological prevention in neointimal formation based on the inflammatory response in vascular neointimal formation.

FGF21, a member of the FGF family, is an endocrine factor secreted into circulation through the liver as an important metabolism regulator [2]. Indeed, FGF21 improves insulin sensitivity, glucose and lipid

* Corresponding author. Department of Clinical Pharmacy, School of Preclinical Medicine and Clinical Pharmacy, China Pharmaceutical University, 24 Tong jia Lane, Nanjing, 210009, China.
E-mail address: mingxu@cpu.edu.cn (M. Xu).

https://doi.org/10.1016/j.atherosclerosis.2019.08.017
Received 23 March 2019; Received in revised form 23 August 2019; Accepted 29 August 2019
Available online 29 August 2019
0021-9150/

homeostasis, and preserves β-cell functions [3]. Thus, FGF21 is thought to be a promising candidate for the treatment of diabetes without hypoglycemia and edema [4]. In addition, FGF21 directly exerts a protective role against myocardial ischemia/reperfusion injury and atherosclerosis [5,6]. VSMCs are dominant cellular constituents of arteries and critical determinants of vascular disease. In diabetic pathological conditions, VSMCs are more prone to proliferation and migration, leading to lumen restenosis and consequently triggering ischemic events. It was reported that FGF21 protected against VSMCs calcification via FGFR1/β-klotho/P38/MAPK/RUNX-2 signaling pathway *in vitro* [7,8]. FGF21 could potentially attenuate the pathogenic destabilization of hypoxia-induced pulmonary hypertension inhibiting the release of TNF-α, IL-1 and IL-6 in pulmonary artery smooth muscle cells [9]. Recently, FGF21 has emerged as a novel regulator preventing cardiac hypertrophic remodeling [10]. Therefore, it is possible that FGF21 prevents diabetes-associated vascular restenosis via a direct action on VSMCs.

Accumulating evidence indicates that vascular inflammation is an important pathogenic factor in diabetes-associated vascular complications [11]. NLRP3 inflammasome contains NLRP3, ASC and caspase-1 as a cytosolic complex for early inflammatory responses [12,13]. Upon activation, NLRP3 forms a complex with its adaptor ASC, which facilitates the conversion of procaspase-1 to active caspase-1. Then, the activated caspase-1 processes pro-IL-1β into its mature form IL-1β and thus triggers an inflammatory response. NLRP3 inflammasome is considered to be involved in the onset of phenotype transformation, proliferation and calcification in VSMCs, which contributes to the pathogenesis of diabetes-associated vascular complications [14–16]. It was reported that the beneficial effects of FGF-21 against diabetes-associated vascular complications depend on inhibiting the activation of NF-κB/NLRP3 inflammasome [17].

Thus, the present study was designed to investigate the potential therapeutic effects of FGF21 in VSMCs proliferation and migration, which was associated with inhibition of NLRP3 inflammasome in diabetes-related vascular restenosis. Moreover, the upstream mechanism of NLRP3 inflammasome activation in VSMCs still remains unknown. Syk is a non-receptor tyrosine kinase, which induces NLRP3 inflammasome activation and IL-1β maturation [18]. Here, Syk dephosphorylation was expected to mediate the inhibition of NLRP3 inflammasome responding to FGF21 treatment in VSMCs.

2. Materials and methods

2.1. Model of diabetic mice

Adult male BALB/c mice, weighing 25–28 g, were obtained from Qinglongshan Lab Animal Ltd, Nanjing, China. Animal handling and experimental procedures were approved by the ethic committee of China Pharmaceutical University, in accordance with the Guidelines of Animal Experiment set by the Bureau of Sciences and Techniques of Jiangsu Province, China [NO. SYXK2007-0025].

The control group mice were fed a normal diet. High fat diet (HFD, 10% saccharose, 10% lard, 10% sugar, 5% egg yolk powder, 0.5% cholesterol, 74.5% basal chow) and low dose of STZ were administered to develop diabetes according to the method described previously [19]. Briefly, after 4 weeks feeding HFD, mice were administered STZ (65 mg/kg body weight, pH 4.5) or citrate buffer (vehicle) by intraperitoneal (i.p.) injections once a day for 5 days. After one week, the mice were fasted for 12 h for testing of fasting blood glucose (FBG) and oral glucose tolerance test (OGTT). OGTT was performed by orally administering 2.0 g/kg D-glucose to overnight-fasted mice. Blood glucose levels were then determined at 0, 30, 60, and 120 min. Plasma glucose concentration was detected using a commercial glucose kit (Jiancheng Bioengineering Institute, Nanjing, China). Fasted mice with blood glucose level higher than 11.1 mmol/L were considered as diabetic mice.

2.2. Wire-mediated vascular injury

Diabetic mice were anesthetized and the surgical procedure was performed as previously described [20]. Briefly, the left common carotid artery (CCA) was dissected and proximally ligated, the external carotid artery and internal carotid artery were also distally ligated. CCA was injured with a flexible wire (0.38 mm diameter) which was inserted from the external carotid artery and passed 8 times in CCA. Following the removal of the wire, the external carotid artery was tied off and the internal carotid artery circulation was restored. After two weeks, the operative mice were divided into two groups, and the diabetic group treated with FGF21 (5 mg/kg/d, intravenous injection) or the same amount of saline injection as negative control. After four weeks, CCAs among all groups were harvested and fixed by 4% paraformaldehyde (PFA, ALADDIN shanghai, China) or frozen directly in liquid nitrogen.

2.3. HE staining of common carotid artery

After deparaffinization and rehydration, CCA sections were dyed with hematoxylin solution (hematoxylin 1 g, sodium iodate 0.2 g, aluminium potassium sulfate, 50 g, citric acid 1 g, chloral hydrate 50 g, distilled water added to 1 L) for 10 min, and then alcoholic eosin (2.5 g eosin, 500 ml distilled water, hydrochloric acid 10 ml, filter product dissolved in 1000 ml 95% alcohol, double diluted before use) for 30 s. The cross-sectional area of media and intima was measured by Image J software (NIH, Littleton, CO, USA) and the intima/media ratios were calculated.

2.4. Vascular tension recording

The constriction function of CCA was detected by tension detection system (BL-420S, TaiMeng, Chengdu, China) as described previously [21,22]. Mice were anaesthetized and CCA was quickly removed and immersed into Krebs Henseleit solution (mM) (KH, pH 7.4, 119.0 NaCl, 25.0 $NaHCO_3$, 11.1 Glucose, 2.4 $CaCl_2$, 4.7 KCl, 1.2 KH_2PO_4, 1.2$MgSO_4$, 0.024 Na_2EDTA). CCA was carefully dissected into a transparent tube, and then cut into vascular rings with a width of approximately 2 mm. The endothelium of CCAs was removed using a flexible wire (0.38 mm diameter). The vascular rings were then suspended in a water-jacketed tissue bath and the tension tested. KH solution was maintained at 37 °C and the mixed gas containing 95% O_2, and 5% CO_2 was continuously bubbled through the bath. The baseline load placed on the rings was 1.0 g. When the tension of the rings was stable at basal level, the rings were contracted with 60 mM KCl to obtain a maximal response, and then a cumulative dose-response curve to phenylephrine (Phe, 1×10^{-9}-10^{-4} M) was conducted.

2.5. Primary VSMC culture

Primary VSMCs were isolated from the thoracic aorta of mice as described previously [23]. VSMCs were cultured in Dulbecco's modified Eagle's medium (DMEM, Giabco, lifetechnologies, China) with 15% fetal bovine serum (FBS, Gibco, lifetechnologies, China), penicillin (100 IU/ml) and streptomycin (100 mg/ml) at 37 °C in a 5% CO_2 humidified incubator. VSMCs in the third to eighth passage were used and cells at 80–90% confluence were blocked by incubation in serum-deprived DMEM for 24 h before intervention.

2.6. VSMCs migration assay

VSMCs were cultured in six-wells plates with normal medium and HG medium until confluence and incubated with serum-deprived normal and HG medium for 12 h. A scratch was gently made using a sterile pipette tip, and the cells were washed and then incubated with FBS-free normal and HG medium with or without FGF21 (Novoprotein, shanghai, China), MCC950 (15 nM, MedChemExpress, USA), Z-WEHD-

FMK (WEHD, 1 mM, ApexBio Technology, USA) and R406 (2.5 mM, MedChemExpress, USA) for 24 h. The images of the wounded area were photographed immediately (time 0) and 24 h after scratch. The wound areas were calculated by image J software (NIH, Littleton, CO, USA). Wound closure was quantified as percentage of initial wound area that had been recovered by VSMCs,% Wound Closure = ($area_{t0}$-$area_{t24}$)/$area_{t0}$ × 100%.

In addition, transwell migration assay was also performed as previously described [24]. Transwell chambers (Costar transwell; Corning, USA) with 8 μm pores were coated with 0.1% gelatin (ALADDIN shanghai, China). FBS-free HG medium was added to the bottom chamber. VSMCs (5×10^4 cells per well) were suspended in 100 μl FBS-free medium and then added to the upper chamber. After 4 h of incubation, cells on the upper surface of the membrane that had not migrated were scraped off with cotton swabs, and cells that had migrated to the lower surface were fixed by 4% PFA and stained with 0.25% crystal violet (ALADDIN shanghai, China). The average number of cells from 3 randomly chosen fields on the lower side of the membrane was counted.

2.7. Zymography

The activity of MMP2 and MMP9 was detected by gelatin zymography assay as described previously [25]. Briefly, serum-starved VSMCs were pretreated with HG for 48 h, and gradient concentration of FGF21 was added for another 24 h. After treatment, the medium supernatant was collected and clarified by centrifugation (8000 *g*, 10 min, 4 °C) and the total protein concentration was measured using Bradford protein assay kit (keygentec, Nanjing, China). The medium was mixed with non-reducing 4 × SDS loading buffer (50 mM Tris-HCl, pH 6.8, 2% SDS, 10% glycerol, 12.5 mM EDTA, 0.02% bromophenol blue) and electrophoresed on a 10% SDS-PAGE gel containing 0.1% gelatin. Separated gels were washed by elution solution (2.5% Triton X-100, 50 mmol/L Tris-HCL, 5 mmol/L $CaCl_2$ and 1 μmol/L $ZnCl_2$, pH 7.6) for 4 times, 15 min each time, to remove SDS in the gel and then rinsed with rinse solution (50 mmol/L Tris-HCL, 5 mmol/L $CaCl_2$, and 1 μmol/L $ZnCl_2$, pH 7.6). The gels were incubated at 37 °C for 48 h for the development of zymolytic bands with incubation solution (50 mmol/L Tris-HCL, 5 mmol/$CaCl_2$, 1 μmol/L $ZnCl_2$ and 0.02% Brij-35, pH 7.6). Protease bands were detected by absence of Coomassie Brilliant Bluer R-250 staining of digested gelatin. The gels were photographed with automatic chemiluminescence/fluorescence image analysis system (5200 Multi, Tanon, shanghai, China).

2.8. Western blot analysis

Western blot analysis was performed as described previously. Briefly, total proteins from VSMCs were extracted using RIPA lysis buffer (Biouniquer, USA). Protein concentration was quantified using a BCA Protein Assay Kit (keygentec, Nanjing, China). According to the quantification, the total protein was adjusted to equal 5 × loading buffer (Biouniquer, USA), and samples were boiled for 5 min at 95 °C. The cell culture medium supernatant was also collected and clarified by centrifugation (8000 *g*, 10 min and 4 °C). According to the quantification, the supernatant was mixed with non-reducing 4 × SDS loading buffer. Equal amounts of cell lysate or supernatant protein were resolved by SDS-PAGE using 5% (w/v) stacking and 10% (w/v) separating polyacrylamide gels, and then transferred to 0.45 μm polyvinylidene difluoride membrane (PVDF, Millipore, USA), which was then blocked for 1.5 h in 5% (w/v) non-fat milk diluted in Tris-buffered saline (TBST, 100 mM Tris-HCL, pH 7.4) with 0.01% (v/v) Tween-20, and incubated with the indicated primary antibodies overnight at 4 °C. The primary antibodies were rabbit anti-NLRP3 (1:1000, Abways Technology, Inc., Shanghai, China), rabbit anti-PYCARD (ASC, 1:500, Abways Technology, Inc., Shanghai, China), rabbit anti-p20 (1:500, Abways Technology, Inc., Shanghai, China), rabbit anti-pSyk-try525 (1:1000, Abways Technology, Inc., Shanghai, China), rabbit anti-IL-1β (1:1000, Abways Technology, Inc., Shanghai, China), rabbit anti-MMP2 (1:1000, Abways Technology, Inc., Shanghai, China), rabbit anti-MMP9 (1:1000, Boster Biological Technology, wuhan, China), rabbit anti-PCNA (1:3000, Abways Technology, Inc., Shanghai, China), rabbit anti-cyclin D1 (1:1000, Abways Technology, Inc., Shanghai, China), rabbit anti-GAPDH (1:5000, Abways Technology, Inc., Shanghai, China). After 3 times of wash, the membranes were incubated with goat anti-rabbit IgG (1:5000, Abways Technology, Inc., Shanghai, China) for 1.5 h. The blot was detected by automatic chemiluminescence/fluorescence image analysis system (5200 Multi, Tanon, shanghai, China) with LumiGlo and Peroxide (1:1, Tanon, shanghai, China). Densitometric analysis of the images was performed with Image J software (NIH, Littleton, CO, USA).

2.9. ASC oligomerization assay

ASC oligomer was detected by ASC oligomer cross-linking using disuccinimidyl suberate (DSS, ALADDIN, shanghai, China) as described previously [26]. VSMCs were treated with lipopolysaccharide (LPS, 1 μg/ml, Sigma-Aldrich, USA) and ATP (5 mM, ALADDIN, shanghai, China) for 4 h, as the positive control of NLRP3 inflammasome activation. VSMCs were lysed on ice in 500 μl of buffer A (20 mM HEPES·KOH, pH 7.5, 10 mM KCl, 1.5 mM $MgCl_2$, 1 mM EDTA, 1 mM EGTA, 320 mM sucrose) after scratching. The cell lysates were centrifuged at 1,800 *g*, 4 °C for 8 min to remove the bulk nuclei. 20 μl supernatant was kept for Western blot assay to test total ASC expression in the cell lysates. The remaining supernatant was diluted with buffer A in a 1:1 ratio and centrifuged for 5 min at 2,000 *g*, 4 °C. After centrifugation, the supernatant was diluted with equal volume of CHAPS buffer (20 mM HEPES·KOH, pH 7.5, 5 mM $MgCl_2$, 0.5 mM EGTA, 0.1 mM PMSF, 0.1% CHAPS) and again centrifuged at 5,000 *g* for 8 min to pellet the ASC oligomers. The pellets were suspended in 50 μl CHAPS buffer with 4 mM DSS which was dissolved in DMSO for 30 min at room temperature to cross-link proteins. After another centrifugation at 5,000 *g*, 4 °C for 8 min, the pellets were suspended in 30 μl 2 × loading buffer (double diluted the 4xprotein loading buffer in distilled water without reducing agent). The samples were boiled for 5 min at 95 °C, and then detected by Western blot assay.

2.10. BrdU incorporation assay

BrdU incorporation assay was performed as described previously [27]. VSMCs were seeded on coverslips in six-well plates with normal and HG medium to 60–70% confluences, and then incubated with serum-deprived normal and HG medium for 12 h. VSMCs were labeled with BrdU (10 μM, Solarbio, Beijing, China) in normal and HG medium with or without FGF21, MCC950, WEHD, R406 and PD173074 (50 nM, MedChemExpress, USA) for 24 h. After fixed by 4% PFA, perforated by 0.3% Triton X-100 and denatured by 2 M HCl, VSMCs were incubated with mouse anti-BrdU primary antibody (1:100, Proteintech™, Wuhan, China) overnight, followed by Cy3–conjugated Goat Anti-mouse IgG (H + L) (1:100, ProteintechTM, Wuhan, China). The immunofluorescence images were taken by Fluorescence microscope (Carl Zeiss, scope A1, Germany). The percentage of BrdU positive cells to the total amount of cells was calculated by image J software (NIH, Littleton, CO, USA).

2.11. Immunofluorescence analysis

VSMCs (5×10^4 cells) were seeded in 35 mm diameter confocal dishes dish. After treatment, cells were washed three times by PBS (137 mM NaCl, 2.7 mM KCl, 10 mM Na_2HPO_4, 1.8 mM KH_2PO_4) and fixed by 4% PFA for 30 min. Cell membrane was perforated by 0.3% Triton X-100 (Biosharp, Hefei, China) for 15 min and cells were blocked with 5% bovine serum albumin (BSA, Solarbio, Beijing, China) for

1.5 h. The primary antibodies, rabbit anti-NLRP3 (1:200, Abways Technology, Inc., Shanghai, China) and rabbit anti- PYCARD (ASC, 1:100, Abways Technology, Inc., Shanghai, China) were incubated for 5 h, respectively. After triple washing, NLRP3 and ASC were labeled by the second fluorescent antibodies Cy3–conjugated Goat Anti-Rabbit IgG(H + L) (1:100, Proteintech™, Wuhan, China) and Goat Anti-Rabbit IgG (H + L) Alexa Fluor 488 (1:100, Abways Technology, Inc., Shanghai, China) for 2 h, respectively.

Optimal cutting temperature compound (OCT, CellPath, U.K.) embedded CCA sections were permeabilized with 0.1% Triton X-100 in PBS after washing the OCT. The sections were fixed and blocked like VSMCs procedure. The sections were incubated with the primary antibodies, rabbit anti-SMA (1:100, Proteintech™, Wuhan, China) and rabbit anti-NLRP3 (1:100, Abways Technology, Inc., Shanghai, China), anti-SMA (1:100, Proteintech™, Wuhan, China) and rabbit anti-PYCARD (ASC, 1:100, Abways Technology, Inc., Shanghai, China) followed by Cy3 and Alexa Fluor 488, respectively.

Fluorescent images were photographed by a Laser scanning confocal microscope (Carl Zeiss, LSM700, Germany) and the images of VSMCs and CCA were processed by ZEN blue 2.3 software (Carl Zeiss, Germany). The Pearson's coefficient which represents col-localization of NLRP3 and ASC was calculated by Image J software (NIH, Littleton, CO, USA).

2.12. Immunohistochemistry

After deparaffinization and rehydration, CCA sections were blocked with 3% hydrogen peroxide (1 ml 30% aquae hydrogenii dioxide, 9 ml methanol) at room temperature for 10 min after antigen retrieval. Sections were blocked with 5% BSA for 10 min. The primary antibodies rabbit anti-p20 (1:100, Abways Technology, Inc., Shanghai, China), rabbit anti-pSyk-try525 (1:100, Abways Technology, Inc., Shanghai, China), rabbit anti-IL-1β (1:100, Abways Technology, Inc., Shanghai, China), rabbit anti-MMP9 (1:50, Boster Biological Technology, wuhan, China), rabbit anti-PCNA (1:200, Abways Technology, Inc., Shanghai, China) were applied for 12 h at 4 °C, followed by the incubation with horseradish peroxidase-conjugated rabbit anti-goat IgG (1:500, Abways Technology, Inc., Shanghai, China) for 30 min at room temperature. 3, 3-Diaminobenzidine (DAB, Beyotime Biotechnology, Shanghai, China) was used to develop the positive cells in CCA. Sections were counterstained with hematoxylin, and then covered with glass coverslips. Optical density values were determined by Image Pro Plus 6.0 software (Media Cybernetics, Inc. USA).

2.13. Statistics

Statistical analysis was performed with IBM SPSS Statistics 20 software. Data are presented as means ± SE. Significant differences between and within multiple groups were examined using ANOVA for repeated measures, followed by Duncan's multiple-range test. The Independent-Samples *t*-test was used to detect significant differences between two groups. $p < 0.05$ was considered statistically significant.

3. Results

3.1. FGF21 ameliorated neointimal hyperplasia and vascular dysfunction

We examined the beneficial effects of FGF21 on neointimal hyperplasia using a wire-injured model in diabetic mice. In HE staining, neointimal hyperplasia was significantly observed in CCA at 4 weeks after wire-mediated vascular injury (Fig. 1A and B). However, neointimal formation was not remarkable in diabetic mice without wire-injury. Quantitative analysis on computerized image system showed that the intima-to-media ratio was significantly reduced in the FGF21-treated group, but not in the saline injection group, which dissolved FGF21 as a negative control. This data suggested that FGF21 effectively inhibited neointimal hyperplasia in wire-injured diabetic mice.

Vascular response to phenylephrine was tested in CCA obtained from the mice. Fig. 1C–E shows the effects of FGF21 on the contractile response to phenylephrine in aortic strips without endothelium. Relative to the control mice, the contractile response to phenylephrine was stronger in the untreated diabetic mice, subjected to wire-injury. The impaired contraction was markedly ameliorated after FGF21 administration. These results imply that FGF21 may relieve endothelium-independent contraction of CCA from diabetic mice with or without wire-injury. In a preliminary experiment, FBG was raised after 4 weeks for HFD feeding (Supplemental Fig. 1). Following injection of STZ in mice with HFD, FBG was significantly elevated relative to the control group (Fig. 1F). After FGF21 administration, FBG was significantly suppressed as well as blood glucose of OGTT, which was conducted based on blood glucose of 0, 30, 60, 90 and 120 min after oral glucose administration in mice (Fig. 1G and H). It also confirms FGF21 as an endocrine regulator of glucose metabolism [28].

Vascular neointimal hyperplasia after vascular injury is mainly characterized by VSMCs proliferation, migration, phenotypic transformation and extracellular matrix collagen deposition [29,30]. Exposure to 30 mM glucose for 48 h in cultured VSMCs increased the expression of PCNA, a typical marker for proliferation (Supplemental Figs. 2A and B). A similar trend was observed in cyclin D1 expression, which regulates cell cycle in mitosis (Supplemental Figs. 2A and C). FGF21 treatment resulted in inhibition of HG-induced expression of PCNA and cyclin D1 proteins in a dose-dependent manner.

Upregulation of metalloproteases, particularly MMP2 and MMP9, has been demonstrated as a driver for vascular neointimal hyperplasia [31]. These enzymes facilitate VSMCs migration at the early stage of neointimal formation and regulate matrix turnover and accumulation during neointimal hyperplasia. By using gelatin zymography and Western blot, we found that the activity and protein levels of MMP2 and MMP9 were significantly elevated in HG-treated VSMCs (Supplemental Figs. 2D–F). Next, wound healing assays (Supplemental Figs. 2G and H) and transwell migration assay (Supplemental Figs. 2I and J) were used to assess cell migration *in vitro*, respectively. Migrated cells in wounded areas and the average number of VSMCs in the lower side of the membrane in the transwell assay were dramatically increased in HG-induced VSMCs. VSMCs migration, along with the activity and protein levels of MMP2 and MMP9, was markedly blocked after treatment with FGF21. Therefore, we assume that FGF21 effect on VSMCs migration may be related to the inhibition of the activity and protein levels of MMP2 and MMP9.

3.2. FGF21 inhibited NLRP3 inflammasome activation in VSMCs

It was reported that NLRP3 inflammasome is activated in the pathologic process of T2DM, and elevated glucose levels may stimulate the formation of NLRP3 inflammasome by triggering oxidative stress and mitochondrial dysfunction [32]. NLRP3 inflammasome is a combination of NLRP3, ASC oligomer and the recruited procaspase-1. In case of NLRP3 inflammasome, ASC oligomerization is the critical step for caspase-1 activation and IL-1β secretion [33]. Consistent with LPS plus ATP, the positive control of NLRP3 inflammasome formation, it was found that NLRP3 expression and ASC oligomer level significantly increased in VSMCs exposed to HG (Fig. 2A–C).

Upon recruitment to an inflammasome complex, caspase-1 is activated and processed into mature caspase-1 p20 subunits and these subunits have been shown to be secreted in culture supernatant [34]. Therefore, we analyzed p20/pro-caspase-1 in cell lysate and secretion of bioactive p20 in culture supernatants by Western blot, which was dramatically induced in VSMCs stimulated with HG (Fig. 2A, D and E). In addition, the activated caspase-1 transforms proIL-1β into IL-1β, which is one of most powerful inflammatory factors. In parallel, activation of caspase-1, IL-1β/proIL-1β in cell lysate and secretion of IL-1β in culture supernatants were significantly elevated (Fig. 2A, F and G).

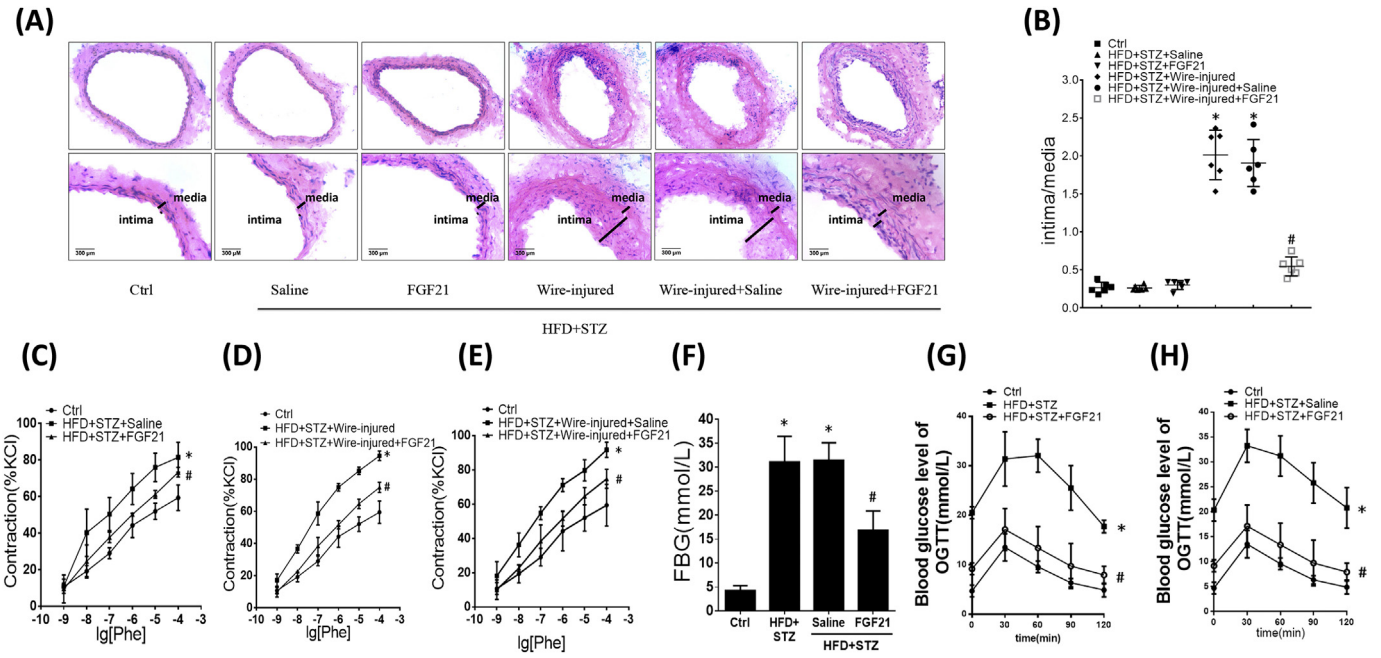

Fig. 1. FGF21 ameliorates neointimal hyperplasia and vascular dysfunction in diabetic mice.
Mice were fed HFD and injected a low dose of STZ (40 mg/kg, i.p.) to develop a diabetic model. Diabetic mice with wire-injured CCA were administered FGF21 (5 mg/kg/d, i.v). Representative images of HE staining show the morphological change (A), and the summarized data show the ratio of intima and media (B). Vascular response to phenylephrine (Phe, 1×10^{-9}-10^{-4} M) was determined in CCA (C–E). The summarized data show the glucose concentration of FBG (F) and OGTT (G and H). $^{*}p < 0.05$ *vs.* Control (Ctrl); $^{\#}p < 0.05$ *vs.* HFD + STZ + Saline mice with or without wire-injured group (n = 6).

Such changes were significantly reversed by FGF21 treatment.

Co-localization of NLRP3 and ASC, the key hallmark of NLRP3 inflammasome activation was detected by immunofluorescence. Yellow punctuates or patches, which merged by red ones (NLRP3) and green ones (ASC) in cytoplasmic regions under the confocal microscope, represented the formation of the NLRP3 inflammasome. Compared with HG and LPS plus ATP treatment, yellow dots were barely detected in VSMCs pretreated with FGF21, showing less NLRP3 inflammasome was assembled due to FGF21 treatment (Fig. 2H and I). Thus, we speculated that FGF21 inhibited the assembly of NLRP3 inflammasome, which finally blocked caspase-1 and IL-1β maturation.

3.3. NLRP3 inflammasome contributed to VSMCs proliferation and migration

To investigate whether NLRP3 inflammasome was associated with HG-induced VSMCs proliferation and migration, VSMCs were treated with a potent and specific NLRP3 inflammasome inhibitor, MCC950 (15 nM, Supplemental Fig. 3) and caspase-1 inhibitor, WEHD (1 mM). As showed in Fig. 4A–E, the expression and secretion of caspase-1 and IL-1β were effectively blocked by MCC950 and WEHD, respectively. It also further demonstrated MCC950 and WEHD as effective inhibitors in the current study. Importantly, MCC950 and WEHD significantly inhibited the expression of PCNA and cyclinD1, as well as MMP2 and MMP9, in VSMCs exposed to HG (Fig. 3A, F-I). Consistently, both the wound healing assays and the transwell migration assay showed that cell migration in HG-induced VSMCs was prevented by MCC950 and WEHD (Fig. 3J-M). However, FGF21 combined with MCC950 or WEHD showed no significantly additive effects on VSMCs proliferation and migration. Therefore, these results indicated that the inhibition of the formation of NLRP3 inflammasome contributed to VSMCs proliferation and migration. The inhibition of NLRP3 inflammasome at least partly accounted for the underlying mechanism that FGF21 inhibited VSMCs proliferation and migration under HG stimulation.

3.4. Syk mediated FGF21-regulated NLRP3 inflammasome in VSMCs

Syk, along with the zeta-chain associated kinase of 70 kDa, is a member of the Syk family of kinases. ASC could be phosphorylated in a Syk-dependent manner at multiple sites, which most likely include Tyr144 essentially required for speck formation [18]. Moreover, the inhibitor of Syk kinase is an effective agent for suppressing VSMCs proliferation and migration and has therapeutic potential for occlusive vascular diseases. Here, VSMCs were treated with R406, a specific small molecule Syk inhibitor, as an anti-inflammatory agent in clinical trials [35]. We found that HG promoted Syk phosphorylation at tyrosine 525/526 in VSMCs, which was suppressed by FGF21 treatment (Fig. 4A and B). As shown in Fig. 5A, C-E, ASC oligomer and p20/pro-caspase-1 were significantly inhibited by R406 similar to FGF21. Moreover, VSMCs proliferation and migration were significantly reversed by R406, as shown in PCNA, cyclinD1, MMP2 and MMP9, as well as the wound healing and transwell assays (Fig.4A, J-M). However, no significant difference of NLRP3 inflammasome activation and VSMC proliferation and migration was found with R406 combined with and without FGF21. Thus, it is suggested that FGF21 inhibited HG-induced Syk phosphorylation at tyrosine 525/526 to prevent NLRP3 inflammasome activation in VSMCs.

It is well-known that FGF21 acts mainly through FGFR1[36], therefore, a potent inhibitor, PD173074, was used to block FGFR1[37, 38]. As shown in Supplemental Figs. 4A–F, Syk phosphorylation, NLRP3 expression, ASC oligomerization, and p20 and IL-1β levels were significantly reversed by FGF21 treatment under HG stimulation. PD173074 abolished the effect of FGF21 on Syk/NLRP3 inflammasome signal. Similarly, Brdu incorporation assay showed that PD173074 blocked the inhibition of FGF21 on VSMCs proliferation under HG condition (Supplemental Figs. 4G–H). Combined with the effects of Syk/NLRP3 inflammasome inhibitors, we further confirmed that the protective effects of FGF21 were associated with Syk/NLRP3 inflammasome signal in HG-impaired VSMCs.

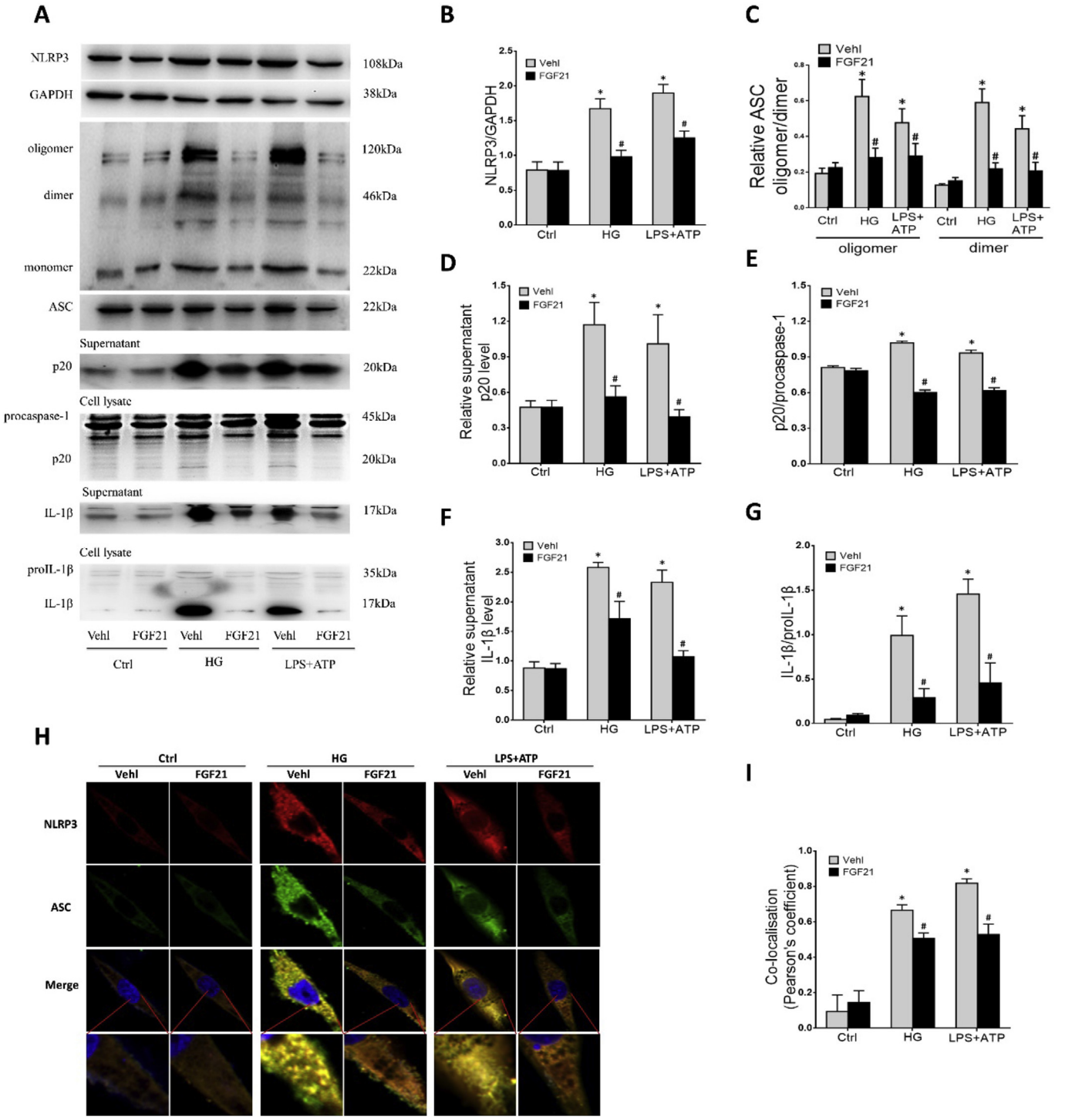

Fig. 2. FGF21 inhibits NLRP3 inflammasome activation in VSMCs.
VSMCs were incubated with HG (30 mM) and LPS plus ATP for 48 h, and treated with FGF21 (200 ng/ml) for 24 h. Representative Western blot gel and summarized data show the protein expression of NLRP3, ASC oligomer, p20 in supernatant, p20/procaspase-1 in cell lysate, IL-1β in supernatant, IL-1β/proIL-1β in cell lysate (A–G). Representative confocal microscopic images and summarized coefficient of colocalization of NLRP3 and ASC (H and I). Yellow spots in the overlaid images were defined as patches colocalization of NLRP3 and ASC. $^{*}p < 0.05$ *vs.* Control (Ctrl); $^{\#}p < 0.05$ *vs.* HG treated group (n = 3). (For interpretation of the references to color in this figure legend, the reader is referred to the Web version of this article.)

3.5. FGF21 inhibited Syk/NLRP3 inflammasome in CCA of diabetic mice

We performed the experiments *in vivo* to determine whether FGF21 prevented vascular Syk/NLRP3 inflammasome activation in CCA from diabetic mice. The immunohistochemical analysis of PCNA and MMP9 was used to examine VSMCs proliferation and migration in the neointima (Fig.5A, E and F). A significantly visible precipitation of PCNA and MMP9 was observed in the arterial media in diabetic mice with or without wire-injury, and a decrease of these proteins could be noted in FGF21-treated mice. Thus, the therapeutic role of FGF21 on neointimal hyperplasia was associated with the down-regulated expression of PCNA and MMP-9 in the artery.

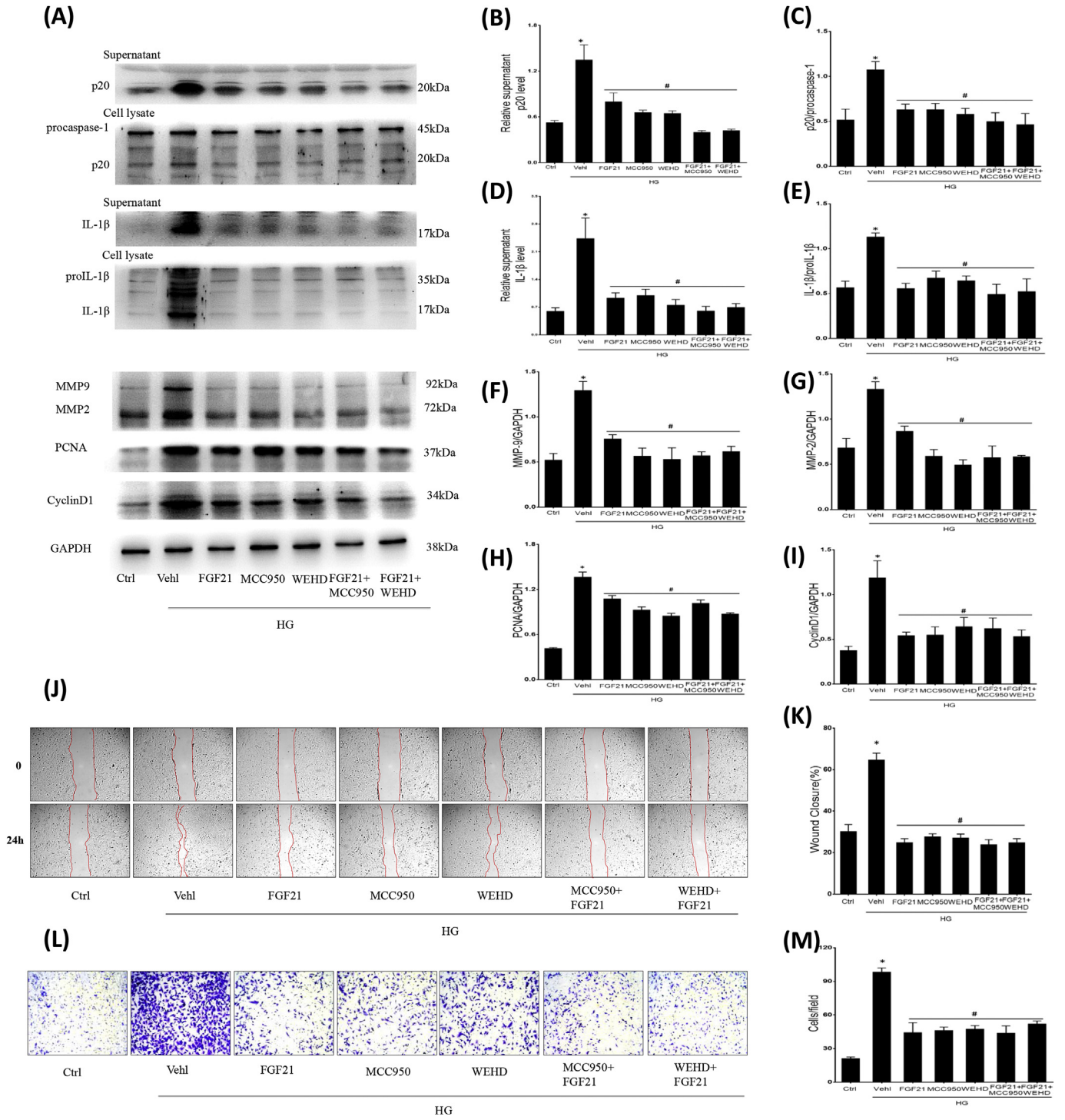

Fig. 3. NLRP3 inflammasome contributes to VSMCs proliferation and migration.
VSMCs were incubated with HG (30 mM) for 48 h, and treated with FGF21 (200 ng/ml), MCC950 (15 nM), WEHD (1 mM), FGF21 + MCC950 or FGF21 + WEHD, respectively, for 24 h. Western blot was used to assesses p20 in the supernatant, procaspase-1 and p20 in the cell lysate, IL-1β in the supernatant, proIL-1β and IL-1β in the cell lysate, MMP2 and MMP9, PCNA and cyclinD1 (A). Summarized results are shown in B–I. The wound healing assays and transwell migration assay were used to test cell migration (J–M). $^{*}p < 0.05$ *vs.* Control (Ctrl); $^{\#}p < 0.05$ *vs.* HG treated group (n = 3).

The immunohistochemical analysis in Fig. 5A revealed that FGF21 could induce a significant reduction in p20 and IL-1β in the neointima in diabetic mice with or without wire-injury, relative to untreated diabetic mice. Using confocal microscopy, co-localization of NLRP3 or ASC *vs.* α-SMA, a typical marker of VSMC, apparently increased in diabetic mice, as shown as yellow color in CCA (Fig. 5G–I). Co-localization of NLRP3 and ASC further confirmed the formation of NLRP3 inflammasomes on the wall of CCA (Fig. 5G and J). FGF21 almost completely blocked the formation of NLRP3 inflammasomes in CCA of diabetic mice. Similar to the *in vitro* results, a decrease of Syk immunostaining intensity was observed in the neointimal layer of CCA from FGF21-treated mice (Fig. 5A). These results are summarized in Fig. 5B–F and suggest that administration of FGF21 has protective effects on vascular neointima hyperplasia, which is associated with

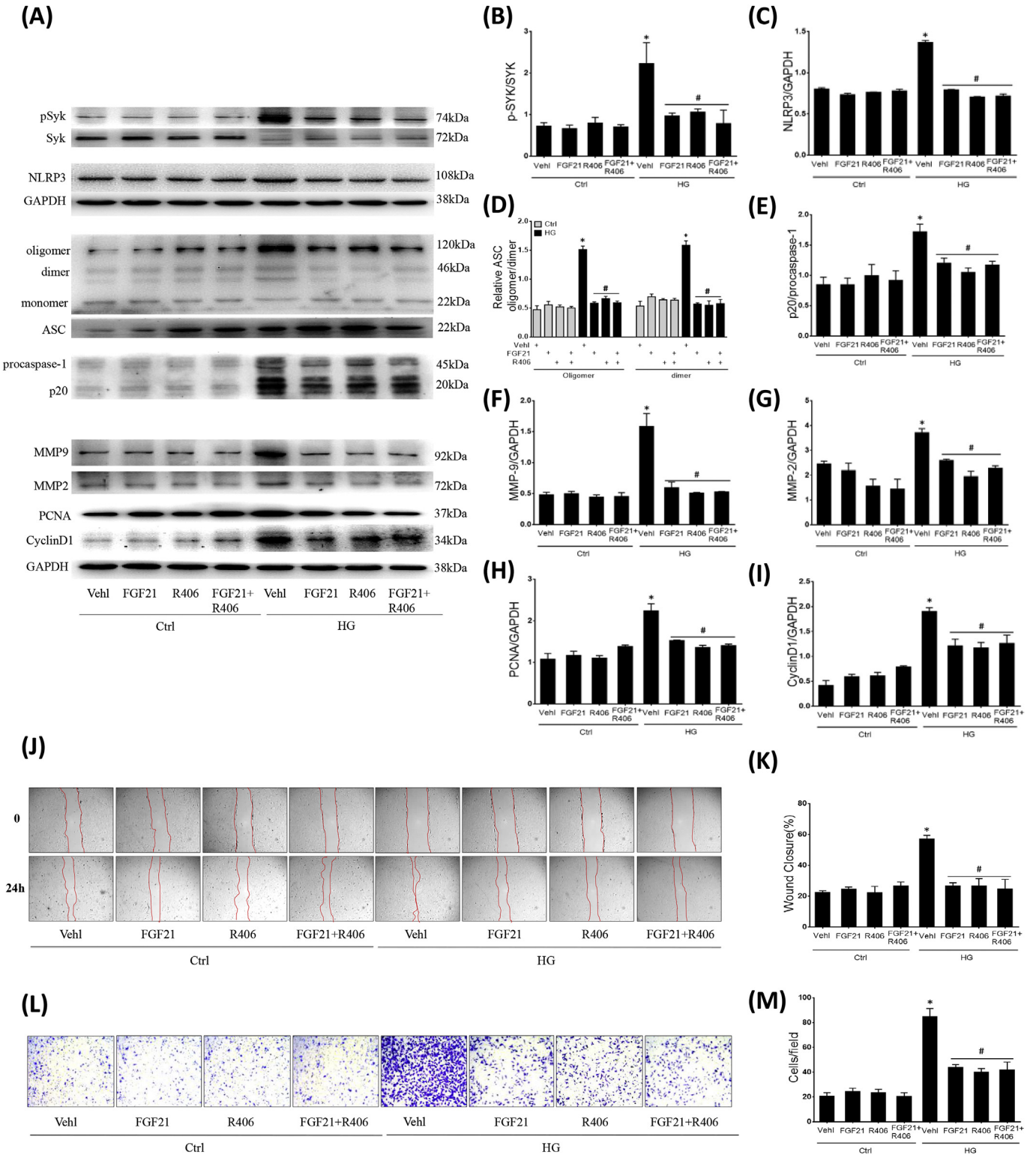

Fig. 4. Syk mediated FGF21-regulated NLRP3 inflammasome in VSMCs.
VSMCs were incubated with HG (30 mM) for 48 h, and treated with FGF21 (200 ng/ml), R406 (2.5 μM), FGF21 plus R406 for 24 h. Western blot was used to assay the protein expression of pSyk/Syk, NLRP3, ASC oligomer, p20/procaspase-1, MMP9, MMP2, PCNA and cyclinD1 (A–I). Typical images and summarized data show cell migration by wound healing assay and transwell assay (J–M). $^{*}p < 0.05$ *vs*. Control (Ctrl); $^{\#}p < 0.05$ *vs*. HG treated group (n = 3).

inhibition of Syk/NLRP3 inflammasome pathway.

4. Discussion

The present study for the first time demonstrated that FGF21 directly inhibited VSMCs proliferation and migration, which lead to restenosis after wire-injury in diabetic mice. Further, we showed that FGF21 inhibited the formation of VSMCs NLRP3 inflammasome through FGFR1 and dephosphorylation of Syk at tyrosine 525 under hyperglycemia stress.

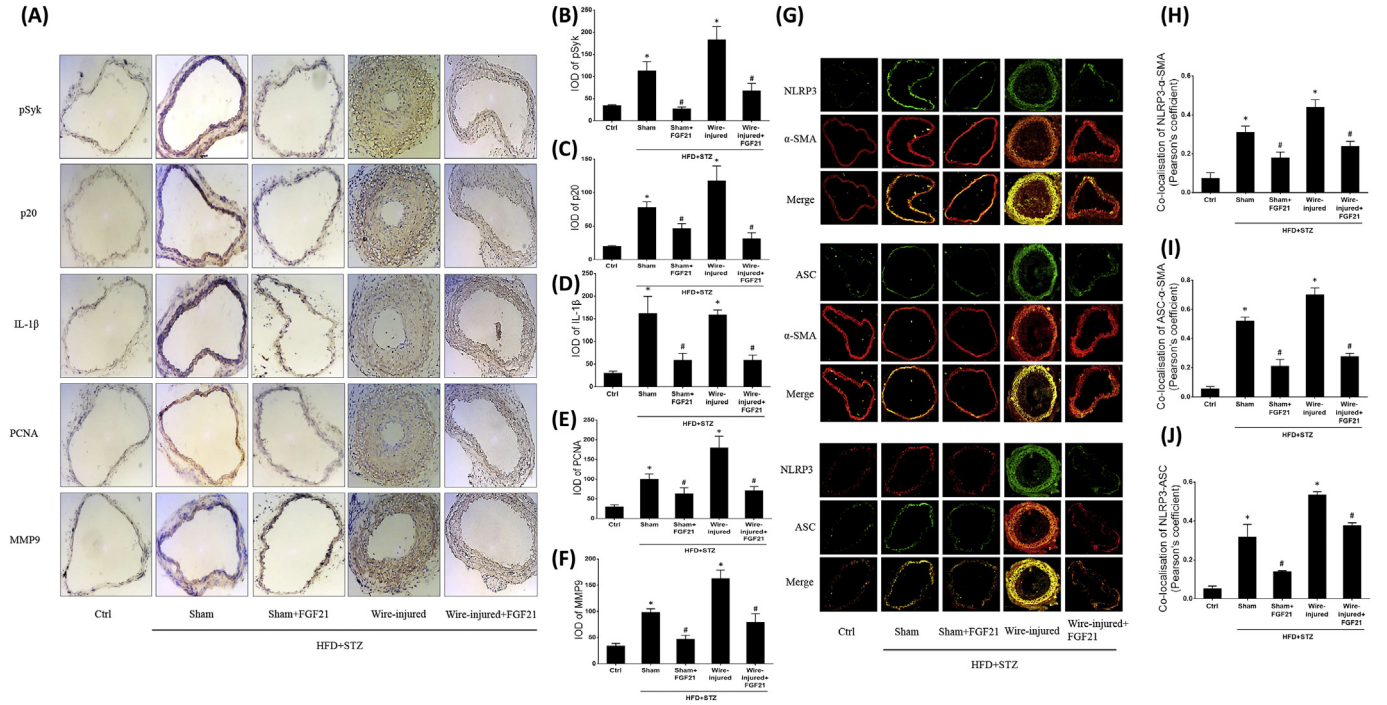

Fig. 5. FGF21 inhibited Syk/NLRP3 inflammasome in CCA in diabetic mice.
Diabetic mice with or without wire-injured CCA were administered FGF21 (5 mg/kg/d, i.v). Representative immunohistochemistry images and summarized integrated optical density (IOD) of pSyk, p20, IL-1β, PCNA and MMP9 (A–F). Typical fluorescent images and summarized Pearson's coefficient show the co-localization of NLRP3/ASC, NLRP3/α-SMA and ASC/α-SMA in CCAs by confocal microscopy (G–J). $^{*}p < 0.05$ *vs*. Control (Ctrl); $^{\#}p < 0.05$ *vs*. HFD + STZ + saline mice with or without wire-injured group (n = 6).

Neointimal formation after vascular injury is the pathological basis of atherosclerosis and restenosis after PCI such as angioplasty and stenting. Many efforts to prevent restenosis have been unsuccessful because of the poor understanding of its pathophysiological mechanism. FGF21 is thought to be an endocrine regulator of glucose and lipid metabolism, which is a critical component for maintaining whole-body homeostasis. Clinical studies have shown that variants of FGF21 have potential to become new drugs for the treatment of T2DM and non-alcohol fatty liver disease [39]. In the current study, we, for the first time, found that FGF21 effectively inhibited neointimal hyperplasia and endothelium-independent contraction in wire-injured CCA from diabetic mice. It has been proved that FGF21 deficiency causes a marked exacerbation of atherosclerotic plaque formation and premature death in apoE knockout mice, and the treatment with recombinant FGF21 reverses the pathological changes [40]. Thus, FGF21 has a protective effect against diabetic vascular complications. It is believed that FGF21 resists atherosclerosis mainly through induction of adiponectin production, which inhibits lipoprotein cholesterol production [41], and further inhibits the migration of VSMCs and blocks macrophage transformation into foam cells [42]. Additionally, some studies have suggested that the improvement of the atherosclerotic pathology by FGF21 is related to the sterol regulatory element binding protein, which is a non-adiponectin pathway to prevent cholesterol synthesis. In addition to its multiple metabolic actions, emerging evidence suggests that FGF21 also has vascular protective activities, independent of its effects on glycemic control and insulin sensitivity. However, it remains unclear whether FGF21 alleviates VSMCs proliferation and migration against vascular neointimal hyperplasia. In the current study, we found that FGF21 indeed inhibited cell proliferation and migration and decreased the expression of PCNA, cyclinD1, MMP2 and MMP9, under high glucose stress. Given some additional mechanisms to regulate VSMCs migration [43,44] and the critical role of MMP in cell migration, we assume that FGF21 effects on VSMCs migration may be related to the inhibition of the activity of MMP2 and MMP9. It was reported that FGF21 prevented calcification *in vitro,* which was associated with blockade of RANK/RANKL/OPG, P38/MAPK/RUNX-2/AMPK and BMP2/Smad signaling pathways [45]. Additional, a study found that FGF21 protected against cerebrovascular aging in human brain vascular smooth muscle cells by improving mitochondrial biogenesis and inhibiting p53 activation in an AMPK-dependent manner [46]. In human coronary smooth muscle cells, the number of HG-induced BrdU positive cells obviously decreased after treatment with FGF21 (Supplemental Fig. 5). Thus, it was suggested that FGF21 has a direct role in VSMCs in addition to its multiple metabolic actions. Recent studies illustrated that FGF21 inhibited Ox-LDL-induced macrophage migration and hypoxia-induced pulmonary artery smooth muscle cells (PASMCs) proliferation by ameliorating inflammatory factors [9,47]. FGF21 inhibitor suppressed proliferation and migration of human umbilical vein endothelial cells through the eNOS/PI3K/AKT pathway [48]. However, other studies showed that FGF21 administration increased the cell migration ability in H9C2 cell line following I/R-induced injury [6]. Treatment with FGF21 promoted cell migration in human fibroblast cells using a wound healing cell migration assay in skin wound healing [49]. Thus, it is assumed that the effects of FGF21 on cell proliferation and migration were dependent on the cell type under different pathological conditions.

Although the pathogenic mechanisms of neointimal hyperplasia have not been completely resolved, an accumulating body of evidence suggests that the inflammatory response plays a key role in the pathological processes. Recently, the reduction of the inflammatory factors, especially IL-1β, by FGF21 was reported by several studies. FGF21 may reduce IL-1β in HFD obese mice and reduce IL-1β transcription induced by Ox-LDL in macrophages and PASMCs [47,50]. The activation of NLRP3 inflammasome leads to the assembly of the multi-protein complex that cleaves and activates caspase-1, resulting in cleavage of pro-IL-1β and release of IL-1β that triggers a downstream inflammatory response. NLRP3 inflammasome could be activated by ROS, cholesterol crystals, and high glucose in diabetes. Our current results show that

FGF21 inhibits NLRP3 expression, ASC oligomerization and co-localization of NLRP3 with ASC. We, for the first time, provided evidence that FGF21 could inhibit NLRP3 inflammasome in diabetic conditions.

Vascular inflammasome activation has been shown to play an important role in vascular remodeling such as atherosclerosis [11]. Here, we demonstrate MCC950 and WEHD prevent VSMCs proliferation and migration, which suggests that NLRP3 inflammasome is possibly involved in vascular neointimal hyperplasia. It was reported that NLRP3 inflammasome activation contributes to VSMCs phenotypic transformation, proliferation and vascular remodeling in hypertension [16]. The activation of the NLRP3 inflammasome mediated inflammatory response pathway is an important step associated with VSMCs calcification induced by β-glycerophosphate [15]. These studies indicate that NLRP3 inflammasome activation contributes to vascular remodeling. Moreover, FGF21 combined with MCC950 and WEHD has no additive effects on VSMCs proliferation and migration, thus, NLRP3 inflammasome is associated with VSMCs proliferation and migration in response to FGF21 treatment.

We further assessed the mechanisms of FGF21-inhibited NLRP3 inflammasome. Syk plays an important role in NLRP3 inflammasome activity by phosphorylation at tyrosine 525/526. Phosphorylation of Syk promotes ASC phosphorylation and oligomerization to form ASC speck, which is one of the inflammasome activating makers [33]. In addition, IL-1β production and release are a Syk-dependent way in antifungal immunity [18]. Syk phosphorylation induced by HG contributes to NLRP3 inflammasome activation in human leukemia monocyte Thp1 cells [51]. Thus, phosphorylation of Syk was expected to connect FGF21 and NLRP3 inflammasome in VSMCs under hyperglycemia. Indeed, we found that Syk phosphorylation is induced by HG along with activation of NLRP3 inflammasome, which is reversed by R406, a typical inhibitor of Syk phosphorylation. Consequently, VSMCs proliferation and migration are attenuated by R406, confirming that Syk regulates the NLRP3 inflammasome in diabetic conditions. This is consistent with a previous report that Syk kinase inhibitor attenuated VSMCs proliferation and migration with or without Ang II stimulation [52,53]. Furthermore, the inhibiting effect of FGF21 on Syk and NLRP3 inflammasome activity was abolished by FGFR signaling blocked by the FGFR1 inhibitor PD173074. To our knowledge, these results, for the first time, provide the evidence that FGF21 could inhibit Syk phosphorylation via FGF21 in VSMCs. It was reported FGF21 plays an important role in anti-inflammation. For example, FGF21 abrogates the increase in TNF-α, IL-1 and IL-6 levels in pulmonary artery smooth muscle cells (PASMCs) culture media and attenuates hypoxia-induced pulmonary hypertension [9]. FGF21 prevents retinal neuronal dysfunction in type 1 diabetic mice, which is associated with reduced IL-1β [54]. Additional evidence demonstrated that FGF21 exerts a direct anti-inflammation role. For example, FGF21 can reduce the expression of IL-1α, IL-6 and TNF-α in Ox-LDL-induced macrophages [47]. FGF21 alleviates arthritis and reduces the expression of IL-17, TNF-α, IL-1β, IL-6, IL-8 in the spleen tissue [55], and reduces the expression of TNF-α, IL-1β, IL-6 and IFN-γ in a dose-dependent manner in LPS-stimulated RAW 264.7 macrophages [56]. Moreover, FGF21 protects IL-1β induced growth retardation in Huh-7 cells. Thus, anti-inflammation was suggested as a critical mechanism underlying FGF21, which provides evidence that Syk and NLRP3 inflammasome constitute a signal pathway and are implicated in the protection of FGF21 in VSMCs remodeling through IL-18 and IL-1β from NLRP3 inflammasome. However, some research showed that high Syk expression promotes expression of MMP2 and MMP9 by activation of the Syk/PI3K pathway in follicular lymphoma cells [57]. Therefore, NLRP3 inflammasome seems not to be one pathway between Syk and MMP2 and MMP9 in different cells, or there is a crosstalk among signal pathways.

Lastly, we confirmed the role of FGF21 and its mechanisms in wire-injured CCA of diabetic mice. Consistent with the *in vitro* results, the immunohistochemical results showed that FGF21 reduces the expression of PCNA and MMP9, p20 and IL-1β as well as Syk phosphorylation at tyrosine 525/526 in diabetic mice. Furthermore, immunofluorescence results showed that FGF21 inhibits co-localization of NLRP3 and ASC in VSMCs in wire-injured and sham diabetic mice, which further confirmed FGF21 inhibits NLRP3 inflammasome in VSMCs. These results suggest that FGF21 ameliorates diabetic vascular neointima hyperplasia by inhibiting Syk/NLRP3 inflammasome in VSMCs.

In conclusion, our data suggest that NLRP3 inflammasome is implicated in VSMCs proliferation and migration in diabetic conditions. FGF21 ameliorates diabetic vascular neointima hyperplasia, which is associated with inhibition of Syk/NLRP3 inflammasome pathway in VSMCs. The present study provides new pharmacological roles and molecular mechanisms of FGF21 on diabetes-related vascular complications.

Conflicts of interest

The authors declared they do not have anything to disclose regarding conflict of interest with respect to this manuscript.

Financial support

This work was supported by the National Natural Science Foundation of China (No. 81570413 and No.81773732 and No.81973509) and Natural Science Foundation of Jiangsu (No. BK20161461).

Author contributions

WW performed the experiments and participated in data analysis and writing of the draft. LXX performed the experiments and participated in the design of the project, XM is responsible for the study design and the revision of the manuscript. All authors read and approved the final manuscript.

Appendix A. Supplementary data

Supplementary data to this article can be found online at https://doi.org/10.1016/j.atherosclerosis.2019.08.017.

References

[1] Z. Qin, K. Zhou, Y.P. Li, et al., Remnant lipoproteins play an important role of in-stent restenosis in type 2 diabetes undergoing percutaneous coronary intervention: a single-centre observational cohort study, Cardiovasc. Diabetol. 18 (2019) 11.
[2] E.M. Domouzoglou, K.K. Naka, A.P. Vlahos, et al., Fibroblast growth factors in cardiovascular disease: the emerging role of FGF21, Am. J. Physiol. Heart Circ. Physiol. 309 (2015) H1029–1038.
[3] B.A. Omar, B. Andersen, J. Hald, et al., Fibroblast growth factor 21 (FGF21) and glucagon-like peptide 1 contribute to diabetes resistance in glucagon receptor-deficient mice, Diabetes 63 (2014) 101–110.
[4] A. Beenken, M. Mohammadi, The FGF family: biology, pathophysiology and therapy, Nat. Rev. Drug Discov. 8 (2009) 235–253.
[5] Z. Lin, X. Pan, F. Wu, et al., Fibroblast growth factor 21 prevents atherosclerosis by suppression of hepatic sterol regulatory element-binding protein-2 and induction of adiponectin in mice, Circulation 131 (2015) 1861–1871.
[6] S. Hu, S. Cao, J. Liu, Role of angiopoietin-2 in the cardioprotective effect of fibroblast growth factor 21 on ischemia/reperfusion-induced injury in H9c2 cardiomyocytes, Exp. Ther. Med. 14 (2017) 771–779.
[7] F. Cao, X. Liu, X. Cao, et al., Fibroblast growth factor 21 plays an inhibitory role in vascular calcification invitro through OPG/RANKL system, Biochem. Biophys. Res. Commun. (2017) 491.
[8] F. Cao, S. Wang, X. Cao, et al., Fibroblast growth factor 21 attenuates calcification of vascular smooth muscle cells inÂ vitro, J. Pharm. Pharmacol. 69 (2017).
[9] J. Liu, G. Cai, M. Li, et al., Fibroblast growth factor 21 attenuates hypoxia-induced pulmonary hypertension by upregulating PPARgamma expression and suppressing inflammatory cytokine levels, Biochem. Biophys. Res. Commun. 504 (2018) 478–484.
[10] A. Kharitonenkov, R. Dimarchi, Fibroblast growth factor 21 night watch: advances and uncertainties in the field, J. Intern. Med. 281 (2017) 233–246.
[11] D. Liu, X. Zeng, X. Li, et al., Role of NLRP3 Inflammasome in the Pathogenesis of Cardiovascular Diseases vol 113, (2017), p. 5.
[12] M.R. de Zoete, N.W. Palm, S. Zhu, et al., Inflammasomes, Cold Spring Harb.

Perspect. Biol. 6 (2014) a016287.
[13] L. Eicke, X. T Sam, S. Andrea, Activation and regulation of the inflammasomes, Nat. Rev. Immunol. 13 (2013) 397.
[14] X.S. Ren, Y. Tong, L. Ling, et al., NLRP3 gene deletion attenuates angiotensin II-induced phenotypic transformation of vascular smooth muscle cells and vascular remodeling, Cell. Physiol. Biochem. Int. J. Exp. Cell. Physiol. Biochem. Pharmacol. 44 (2017) 2269.
[15] C. Wen, X. Yang, Z. Yan, et al., Nalp3 inflammasome is activated and required for vascular smooth muscle cell calcification, Int. J. Cardiol. 168 (2013) 2242–2247.
[16] H.J. Sun, X.S. Ren, X.Q. Xiong, et al., NLRP3 inflammasome activation contributes to VSMC phenotypic transformation and proliferation in hypertension, Cell Death Dis. 8 (2017) e3074.
[17] M.H. Liu, FGF-21 alleviates diabetes-associated vascular complications: inhibiting NF-kappaB/NLRP3 inflammasome-mediated inflammation? Int. J. Cardiol. 185 (2015) 320–321.
[18] A. Mócsai, J. Ruland, V.L. Tybulewicz, The SYK tyrosine kinase: a crucial player in diverse biological functions, Nat. Rev. Immunol. 10 (2010) 387.
[19] S. Peng, P. Wei, Q. Lu, et al., Beneficial effects of poplar buds on hyperglycemia, dyslipidemia, oxidative stress, and inflammation in streptozotocin-induced type-2 diabetes, J. Immunol. Res. 2018 (2018) 7245956.
[20] X. Ning, C. Min, R. Dai, et al., SRSF1 promotes vascular smooth muscle cell proliferation through a Δ133p53/EGR1/KLF5 pathway, Nat. Commun. 8 (2017) 16016.
[21] Q. Li, J. Su, S.J. Jin, et al., Argirein alleviates vascular endothelial insulin resistance through suppressing the activation of Nox4-dependent O2(-) production in diabetic rats, Free Radical Biol. Med. 121 (2018) 169–179.
[22] X.R. An, X. Li, W. Wei, et al., Prostaglandin E1 inhibited diabetes-induced phenotypic switching of vascular smooth muscle cells through activating autophagy, Cell. Physiol. Biochem.: Int. J. Exp. Cell. physiol. Biochem. Pharmacol. 50 (2018) 745–756.
[23] J.L. Ray, R. Leach, J.M. Herbert, et al., Isolation of vascular smooth muscle cells from a single murine aorta, Methods Cell Sci.: Off. J. Soc. In vitro Biol. 23 (2001) 185–188.
[24] E.S. Park, K.P. Lee, S.H. Jung, et al., Compound K, an intestinal metabolite of ginsenosides, inhibits PDGF-BB-induced VSMC proliferation and migration through G1 arrest and attenuates neointimal hyperplasia after arterial injury, Atherosclerosis 228 (2013) 53–60.
[25] H.S. Park, K.T. Quan, J.H. Han, et al., Rubiarbonone C inhibits platelet-derived growth factor-induced proliferation and migration of vascular smooth muscle cells through the focal adhesion kinase, MAPK and STAT3 Tyr 705 signalling pathways, Br. J. Pharmacol. 174 (2017) 4140–4154.
[26] M.A. Di, G. Frera, J. Lugrin, et al., AIM2 inflammasome is activated by pharmacological disruption of nuclear envelope integrity, Proc. Natl. Acad. Sci. U.S.A. 113 (2016) E4671.
[27] D. Liu, Y. Huang, D. Bu, et al., Sulfur dioxide inhibits vascular smooth muscle cell proliferation via suppressing the Erk/MAP kinase pathway mediated by cAMP/PKA signaling, Cell Death Dis. 5 (2014) e1251.
[28] Z. Huang, A. Xu, B.M. Cheung, The potential role of fibroblast growth factor 21 in lipid metabolism and hypertension, Curr. Hypertens. Rep. 19 (2017) 28.
[29] M.R. Bennett, S. Sinha, G.K. Owens, Vascular smooth muscle cells in atherosclerosis, Circ. Res. 118 (2016) 692–702.
[30] M.Y. Jun, R. Karki, K.R. Paudel, et al., Alkaloid rich fraction from Nelumbo nucifera targets VSMC proliferation and migration to suppress restenosis in balloon-injured rat carotid artery, Atherosclerosis 248 (2016) 179–189.
[31] A.C. Newby, Dual role of matrix metalloproteinases (matrixins) in intimal thickening and atherosclerotic plaque rupture, Physiol. Rev. 85 (2005) 1–31.
[32] K. Schroder, R. Zhou, J. Tschopp, The NLRP3 inflammasome: a sensor for metabolic danger? Science 327 (2010) 296–300.
[33] F. Hoss, J.F. Rodriguezalcazar, E. Latz, Assembly and regulation of ASC specks, Cell. Mol. Life Sci. 74 (2016) 1211.
[34] E.I. Elliott, F.S. Sutterwala, Initiation and perpetuation of NLRP3 inflammasome activation and assembly, Immunol. Rev. 265 (2015) 35–52.
[35] G. Olaf, P. Hendrik, B. Michael, et al., Syk kinase signalling couples to the Nlrp3 inflammasome for anti-fungal host defence, Nature 459 (2009) 433.
[39] C. Degirolamo, C. Sabbà, A. Moschetta, Therapeutic potential of the endocrine fibroblast growth factors FGF19, FGF21 and FGF23, Nat. Rev. Drug Discov. 15 (2016) 51–69.
[40] Z. Lin, X. Pan, F. Wu, et al., Fibroblast growth factor 21 prevents atherosclerosis by suppression of hepatic sterol regulatory element-binding protein-2 and induction of adiponectin in mice, Circulation 131 (2015) 1861.
[41] M. L-L, D. Duma, M. Hałabiś, et al., Fibroblast growth factor 21 - a key player in cardiovascular disorders? Horm. Mol. Biol. Clin. Investig. (2016) 30.
[42] L. Jin, Z. Lin, A. Xu, Fibroblast growth factor 21 protects against atherosclerosis via fine-tuning the multiorgan crosstalk, Diabetes Metabol. J. 40 (2016) 22.
[43] H.C. Williams, A. San Martin, C.M. Adamo, et al., Role of coronin 1B in PDGF-induced migration of vascular smooth muscle cells, Circ. Res. 111 (2012) 56–65.
[44] T. Ashino, V. Sudhahar, N. Urao, et al., Unexpected role of the copper transporter ATP7A in PDGF-induced vascular smooth muscle cell migration, Circ. Res. 107 (2010) 787–799.
[45] F. Cao, X. Liu, X. Cao, et al., Fibroblast growth factor 21 plays an inhibitory role in vascular calcification *In vitro* through OPG/RANKL system, Biochem. Biophys. Res. Commun. 491 (2017) 578–586.
[46] X.M. Wang, H. Xiao, L.L. Liu, et al., FGF21 represses cerebrovascular aging via improving mitochondrial biogenesis and inhibiting p53 signaling pathway in an AMPK-dependent manner, Exp. Cell Res. 346 (2016) 147–156.
[47] N. Wang, J.Y. Li, S. Li, et al., Fibroblast growth factor 21 regulates foam cells formation and inflammatory response in Ox-LDL-induced THP-1 macrophages, Biomed. Pharmacother. 108 (2018) 1825–1834.
[48] Y. Li, J. Huang, Z. Jiang, et al., FGF21 inhibitor suppresses the proliferation and migration of human umbilical vein endothelial cells through the eNOS/PI3K/AKT pathway, Am. J. Tourism Res. 9 (2017) 5299–5307.
[49] X. Wang, Y. Zhu, C. Sun, et al., Feedback activation of basic fibroblast growth factor signaling via the Wnt/beta-catenin pathway in skin fibroblasts, Front. Pharmacol. 8 (2017) 32.
[50] Q. Wang, J. Yuan, Z. Yu, et al., FGF21 Attenuates High-Fat Diet-Induced Cognitive Impairment via Metabolic Regulation and Anti-inflammation of Obese Mice vol 55, (2018), pp. 4702–4717.
[51] P.B. Pal, H. Sonowal, K. Shukla, et al., Aldose reductase mediates NLRP3 inflammasome-initiated innate immune response in hyperglycemia-induced Thp1 monocytes and male mice, Endocrinology 158 (2017) 3661–3675.
[52] H.H. Seo, S.W. Kim, C.Y. Lee, et al., A spleen tyrosine kinase inhibitor attenuates the proliferation and migration of vascular smooth muscle cells, Biol. Res. 50 (2017) 1.
[53] B.E. Mugabe, F.A. Yaghini, C.Y. Song, et al., Angiotensin II-induced migration of vascular smooth muscle cells is mediated by p38 mitogen-activated protein kinase-activated c-Src through spleen tyrosine kinase and epidermal growth factor receptor transactivation, J. Pharmacol. Exp. Ther. 332 (2010) 116–124.
[54] Z. Fu, Z. Wang, C.H. Liu, et al., Fibroblast growth factor 21 protects photoreceptor function in type 1 diabetic mice, Diabetes 67 (2018) 974–985.
[55] S.M. Li, Y.H. Yu, L. Li, et al., Treatment of CIA mice with FGF21 down-regulates TH17-IL-17 Axis, Inflammation 39 (2016) 309–319.
[56] Y. Yu, J. He, S. Li, et al., Fibroblast growth factor 21 (FGF21) inhibits macrophage-mediated inflammation by activating Nrf2 and suppressing the NF-kappaB signaling pathway, Int. Immunopharmacol. 38 (2016) 144–152.
[57] S. Fruchon, S. Kheirallah, T. Al Saati, et al., Involvement of the Syk-mTOR pathway in follicular lymphoma cell invasion and angiogenesis, Leukemia 26 (2012) 795–805.